# Physics-based auralization of wind turbine noise

David Mascarenhas, Benjamin Cotté, Olivier Doaré

## HAL Id: hal-03389024
## https://hal.science/hal-03389024

Submitted on 20 Oct 2021

# Physics-based auralization of wind turbine noise

**David Mascarenhas, Benjamin Cotté, Olivier Doaré**
**Institute of Mechanical Sciences and Industrial Applications (IMSIA), ENSTA Paris, CNRS, CEA, EDF, Institut Polytechnique de Paris, France**
**david.mascarenhas@ensta-paris.fr**

## Summary

Amplitude modulation of wind turbine noise is known to be a potential source of annoyance for people living in the vicinity of wind farms. To better understand this auditory annoyance, we propose to auralize the sound that is generated by the wind turbines, rather than to observe a visual representation of the sound levels. It is desirable for the developed auralization tool to be physically-based rather than sample-based. This allows control over the prevailing physical parameters. In our work, the auralization tool is based on Amiet's theory in the frequency domain, and considers the main broadband aerodynamic noise sources, namely trailing edge noise and turbulent inflow noise. For the auralization of the full wind turbine noise, the power spectral density for each blade segment and each position is considered along with the appropriate time shift due to the propagation between the moving blades and the fixed observer. In this study, an efficient method is discussed for the conversion of the frequency-domain power spectral density into a time domain signal. The appropriate time delay due to propagation is accounted for. Finally, a proper implementation of energy conserving cross-fading between consecutive signal grains is proposed. The complete auralized signal for the wind turbine noise in free field is then computed with different receiver orientations and meteorological conditions and compared with the original results in the frequency domain. This auralization tool combined with Virtual Reality/ Augmented Reality can help in building the wind farms while also accounting for auditory annoyance factor in the design phase.

## 1. Introduction

Noise from modern wind turbines is dominated by broadband aeroacoustic mechanisms generated by the wind interacting with the rotating blades. The amplitude modulation of this broadband noise is known to be a potential source of annoyance for people living in the vicinity of wind farms. The

main sources of the broadband noise are to turbulent inflow noise (TIN), trailing edge noise (TEN) and stall noise (Bowdler and Leventhall (2011); Oerlemans and Schepers (2009); Bertagnolio et al. (2017); Buck et al. (2018)). Among these noise sources, stall noise is the most intense and is caused only when the angle of attack of the blade is large, whereas TIN and TEN occur for all angles of attack. Thus, in the simplest case scenario it can be said that TIN and TEN are observed at all times for an operating wind turbine and are the dominant sources of wind turbine noise. The synthesis of these noise sources allows to understand the auditory perception and psychoacoustics that relates to the annoyance caused by the wind turbine noise. Sample-based auralization previously done for wind turbine noise covers a few prevailing parameters and cannot be extended further to compensate for other settings (Pieren et al. (2014)). This restriction occurs because the sample-based synthesis is directly dependent on the noise recordings. There is hence a need for a physics-based auralization, as it allows for a greater control over the desired physical parameters that contribute to the noise generating acoustics. Such an auralization tool can be useful to study the noise generation in the design phase itself and can also helpful to predict the generation of the wind turbine noise in the vicinity.

The frequency-domain modelling of the wind turbine noise sources is studied by Tian and Cotté (2016) based on Amiet's theory (1975; 1976) for TIN and TEN. This noise prediction model is used as the base physical model for the auralization. The main objective of the article is to discuss an auralization tool which converts the frequency-domain model into a time-domain signal, while also accounting for appropriate physical parameters such as time delay due to propagation and geometrical spreading. The two noise mechanisms are presumed to be uncorrelated and are synthesized separately. The resulting synthesized signal is thus a summation of the TIN and TEN, generated by the wind turbine blades in rotation that is experienced by an observer in the free field.

The paper first explains briefly the frequency-domain prediction models for TIN and TEN with few important parameters. The conversion of the frequency spectra to the time-domain signal is explained followed by the description of how the propagation delay is accounted for. Some crucial parameters which are subjective but essential for the auralization are studied in detail. The final auralization tool is presented with a few test cases and the auralized signal are available here: `http://sites.google.com/view/david-mascarenhas/wtnc-2021`.

## 2. Frequency-domain modelling of broadband airfoil noise

For a fixed airfoil of span $L$ and chord $c$, the original models proposed by Amiet (1975; 1976) predict the noise generated by the leading edge and trailing edge of the airfoil assimilated to a thin plate interacting with the turbulent gusts of uniform velocity. The noise observed in the far field $(x_R, y_R, z_R)$ is predicted in the form of a Power Spectral Density (PSD).

### 2.1 Turbulent inflow noise (TIN)

The atmospheric turbulence convected at the inflow velocity $U$, interacting with the leading edge of the airfoil produces turbulent inflow noise. The PSD of the turbulent inflow noise observed in the far-field for an airfoil of large aspect ratio ($L > 3c$), is given by (Amiet (1975); Roger and Moreau (2010)):

$$S_{pp}'^{\text{TIN}}(x_R, y_R, z_R, \omega) = \left(\frac{\rho_0 k c z_R}{2S_0^2}\right)^2 \pi U \frac{L}{2} \Phi_{ww}\left(\frac{\omega}{U}, \frac{ky_R}{S_0}\right)\left|\mathcal{L}_{TI}\left(x_R, \frac{\omega}{U}, \frac{ky_R}{S_0}\right)\right|^2, \qquad (1)$$

where $\omega$ is the angular frequency, $k = \omega/c_0$ is the acoustic wavenumber, $\rho_0$ is the air density, $c_0$ is the speed of sound, $S_0$ is a modified distance between the source and the observer, and $\mathcal{L}_{TI}$ is the turbulent inflow noise transfer function, connecting the airfoil surface pressure fluctuation to the

acoustic pressure at the far-field point. $\Phi_{ww}$ is the two-dimensional energy spectrum, modeled by a von Kármán spectrum for homogeneous and isotropic turbulence (Amiet (1975); Tian and Cotté (2016)).

## 2.2 Trailing edge noise (TEN)

The turbulent boundary layer fluctuations convected at the velocity $U_c$ interact with the trailing edge of the airfoil and generate trailing edge noise. The PSD of trailing edge noise observed in the far-field for an airfoil of large aspect ratio ($L > 3c$), is given by (Amiet (1976); Roger and Moreau (2010)):

$$S'^{\text{TEN}}_{pp}(x_R, y_R, z_R, \omega) = \left(\frac{kcz_R}{4\pi S_0^2}\right)^2 \frac{L}{2} \Phi_{pp}(\omega) l_y\left(\omega, \frac{ky_R}{S_0}\right) \left|\mathcal{L}_{TE}\left(x_R, \frac{\omega}{U_c}, \frac{ky_R}{S_0}\right)\right|^2, \qquad (2)$$

where $\Phi_{pp}$ is the wall pressure fluctuation spectrum, $l_y$ is the spanwise correlation length estimated by the Corcos model, and $\mathcal{L}_{TE}$ is the transfer function for trailing edge noise. The wall pressure fluctuation spectrum $\Phi_{pp}$ is calculated using Goody's model for the pressure side and Rozenberg's model for the suction side of the airfoil (Tian and Cotté (2016)).

## 2.3 Extension to a full size modern wind turbine

By dividing a wind turbine blade into segments with the appropriate aspect ratio and twist, Tian and Cotté (2016) extended these models to a full size wind turbine as can be seen in Fig.1a. As a rotating blade experiences non-uniform flow along the span, with the incoming velocity strongest at the blade tip, the segmentation of the blade allows for the implementation of different inflow velocities for each segment. The segmentation is done ensuring the segment span is greater than the spanwise turbulence correlation length.

To account for the rotational motion of the blade, the model approximates the complete rotation of the blade as a series of translations between discrete angular positions. The convective amplification and Doppler effect caused by the rotating blades is also accounted for following Sinayoko et al. (2013). The instantaneous PSD, $S_{pp}(x_0, \omega, \beta)$ at the observer for an azimuthal blade position $\beta$ is given by:

$$S_{pp}(\mathbf{x_0}, \omega, \beta) = \left(\frac{\omega_e}{\omega}\right) S'_{pp}(\mathbf{x}, \omega_e, \beta), \qquad (3)$$

where $S'_{pp}(\mathbf{x}, \omega_e, \beta)$ given by Eq. (1) and (2) is the PSD for a fixed blade, $\omega_e$ and $\omega$ are the emitted and observed frequencies, $\mathbf{x_0}$ and $\mathbf{x}$ are the observer coordinates in the hub and blade coordinate systems.

The wind profile power law relation $U(z) = U_{ref}(z/z_{ref})^\alpha$ is implemented to consider the influence of different wind inflow velocities at different heights of the atmosphere. The reference inflow velocity $U_{ref}$ = 8 m/s is taken at the hub height $H_0$ = 80 m, chosen as the reference height $z_{ref}$. The implemented source model of Tian and Cotté (2016) for a full size wind turbine thus gives the frequency-domain response of each segment of each blade at each discrete angular position $\beta$ (Fig.1a). This response is obtained for an observer at a position defined by the angle $\tau$ with respect to the wind direction and by the horizontal distance $R_0$ from the base of the wind turbine tower (Fig.1b).

# 3. Auralization method

As each of the segments of the wind turbine blades contribute individually to the total noise, they can be synthesized separately and then summed together at each time step. The synthesis of one
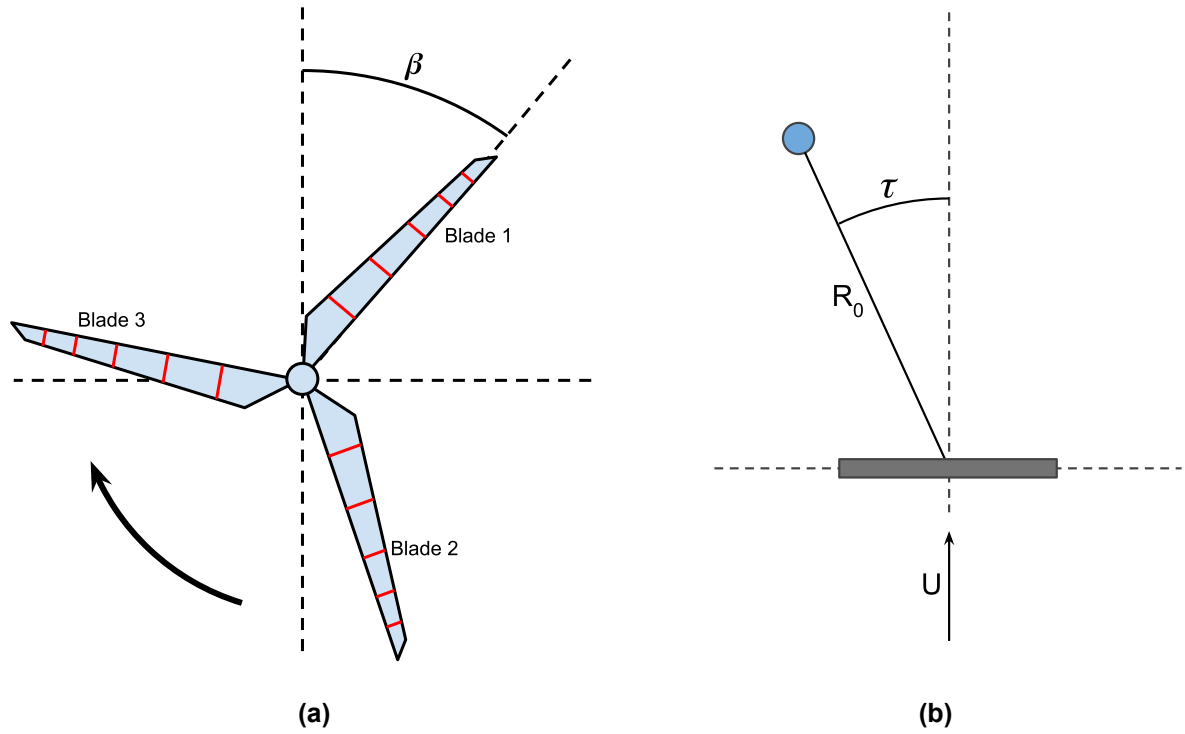
**Figure 1:** (a) Approximated segmentation of the blades and discrete angular position $\beta$ (b) Observer position with respect to the wind turbine rotational plane (top view). $R_0$ is the horizontal distance between the wind turbine hub and the observer, $\tau$ is the angle made by $R_0$ and the wind direction.

segment at a particular blade angular position is referred here as a grain. The noise observed at the receiver is the summation of all the uncorrelated grains at the corresponding time step. We first discuss in Section 3.1 an efficient method to auralize a single grain, which consists in converting the PSD to a time-domain signal. The propagation delay is accounted for in Section 3.2, and the choice of the cross-fading window function is discussed in Section 3.3.

## 3.1 Conversion from frequency spectra to time-domain signal

The PSD in the model of Tian and Cotté is a numerical approximation of the airfoil noise for a set of frequencies. The pressure amplitude corresponding to a particular frequency can be directly calculated as:

$$p(f) = \sqrt{1\text{ Hz} \cdot S_{pp}(f)} \qquad (Pa). \tag{4}$$

This conversion for the all of the frequencies, gives the pressure amplitude-spectra correspondingly. The inverse Discrete Fourier transform (IDFT) converts a frequency-domain spectra into a time domain signal, while conserving the same number of points. The number of points of the concerned pressure amplitude spectrum is insufficient to obtain a time signal of sufficient length. To obtain the desired duration of the signal, the amplitude spectrum is interpolated between the two frequency limits, while the pressure amplitudes for the other frequencies are taken as zero. The total number of frequency points that include the interpolated amplitude spectrum and the frequencies with zero amplitude corresponds to the number of points of the one-sided frequency spectra. As the noise is assumed to be stochastic, a random phase between 0 and $2\pi$ is assigned to each of the complex amplitudes in this one-sided frequency spectrum. To obtain a real-valued signal, the one-sided frequency spectrum is converted to a symmetric double-sided frequency spectrum and the IDFT is taken. The schematic approach of the method is shown in Fig.2a.
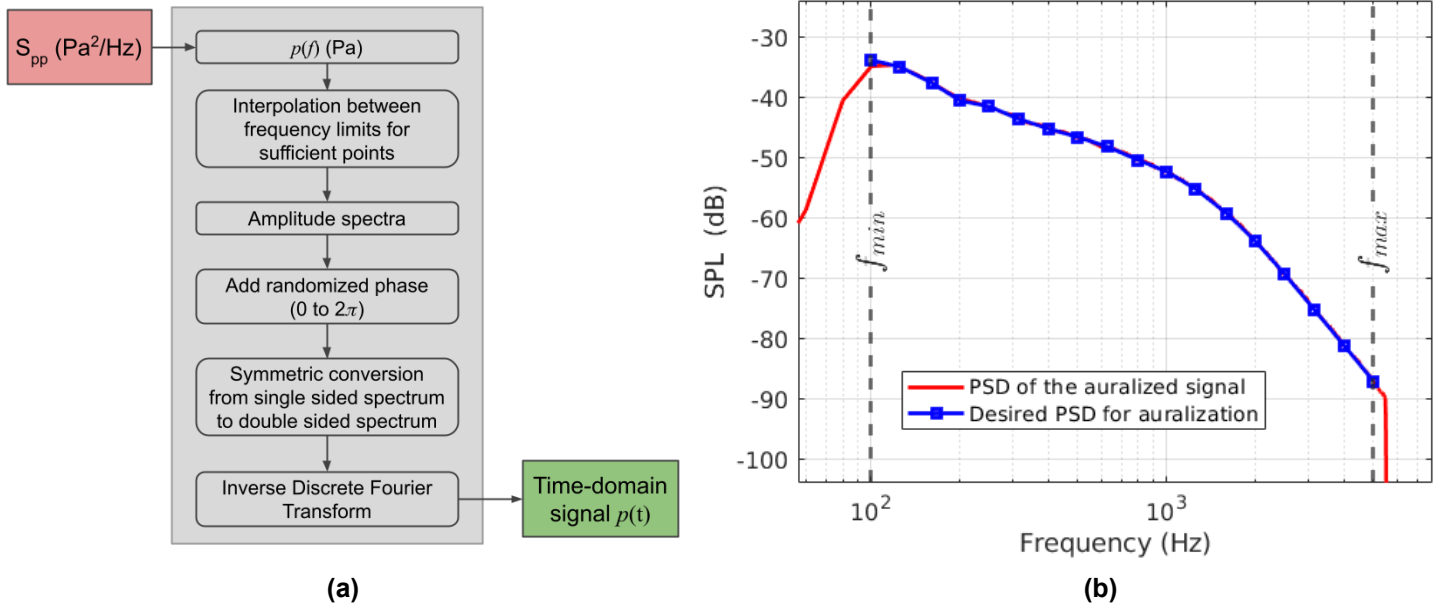
**Figure 2:** (a) Schematic approach of the method for the conversion from the frequency-domain PSD to the time-domain signal, (b) PSD of the resultant auralized grain along with the desired PSD

To avoid edge effects which are observed due to the IDFT, the signal is synthesized to an extraneous length and the truncated to the desired length. This synthesized signal which is obtained from the PSD corresponding to one segment is the grain under consideration. A grain auralized between $f_{min}$= 100 Hz and $f_{max}$= 5000 Hz shows a good replication of the desired PSD as seen in Fig.2b. Beyond the limits of the frequency range set by $f_{min}$ and $f_{max}$ there is a smooth decay of the amplitude of the auralized signal.

## 3.2  Propagation time and grain length

As the rotation of the blades is discretized into a number of angular positions of equal angular steps $\Delta\beta$, the time duration of a single angular step is given by:

$$\Delta t_s = \frac{\Delta\beta}{\Omega},\tag{5}$$

where $\Omega$ is the rotational speed of the wind turbine blade. Depending on the position of the receiver, the propagation distance is different for each segment of the blade at each angular position $\beta$. If the distance between the source and the receiver is $R(\beta)$, then the propagation time is $R(\beta)/c_0$. The time duration of the emitted noise at the receiver is thus given by:

$$T_{\Delta\beta} = \Delta t_s + \frac{\Delta R}{c_0} = \frac{\Delta\beta}{\Omega} + \frac{\Delta R}{c_0},\tag{6}$$

where, $\Delta R = R(\beta + \Delta\beta) - R(\beta)$ is the difference between the propagation distances related to the corresponding successive angular positions that can be positive or negative.

## 3.3  Cross-fading window function

Successive allocation of the auralized grains is observed to produce artifacts in the form of clicks during the transition of one grain to another (Fig: 3a). To avoid this form of artifact, the transition between grains has to be done with a certain amount of overlap between each grain, while still
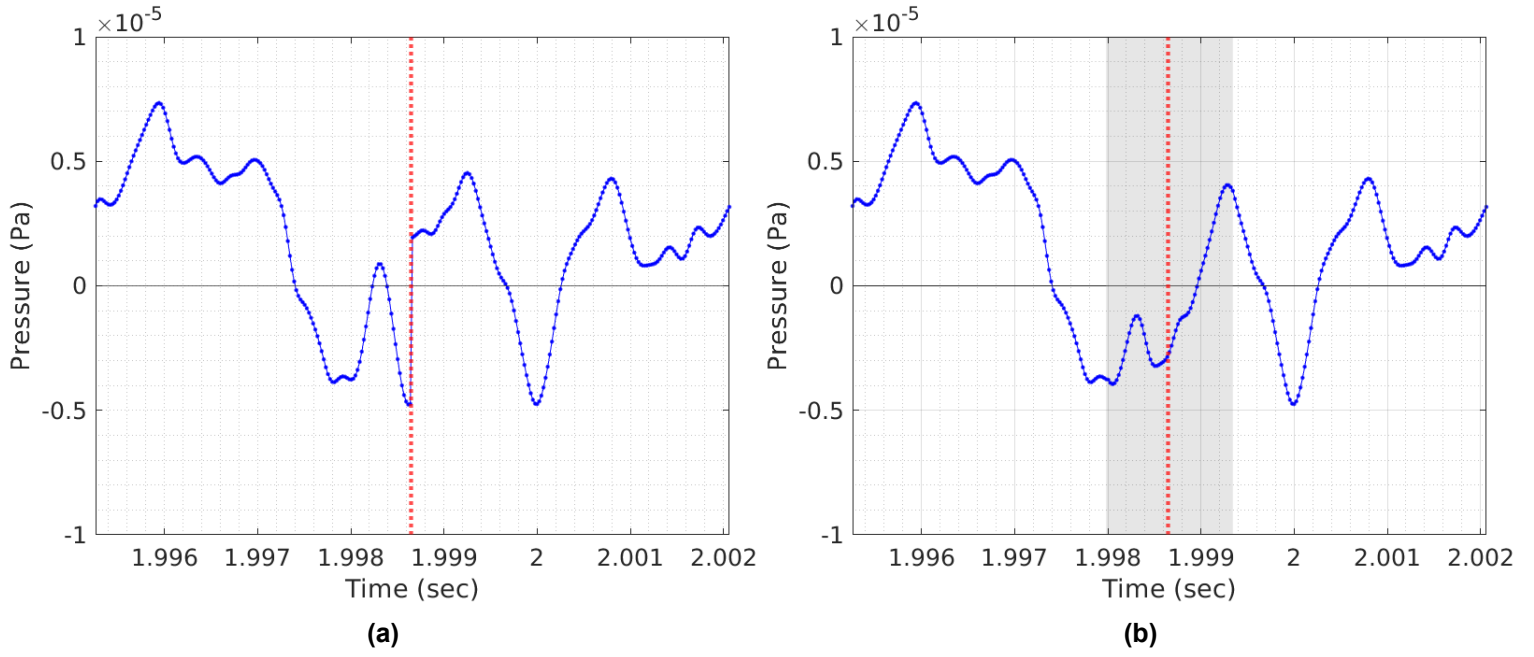
**Figure 3:** (a) Signal without an overlapping window function. Artifacts in the form of clicks are observed at the transitions. (b) Signal with an overlapping window function applied to the shaded region.

conserving the absolute size of each grain. Such transitions of audio signals are known as cross-fading. To facilitate the cross-fading between two grains, a window function is designed and applied to each grain. The window function $W[k]$ of $N$ samples is composed of the overlapping functions $f[k]$ and $g[k]$ with a unit response between them and can be defined as:

$$W[k] = \begin{cases} f[k] & \text{for} \quad 1 \leq k < w_l \\ 1 & \text{for} \quad w_l \leq k \leq N - w_l \\ g[k] & \text{for} \quad N - w_l < k \leq N \end{cases} \qquad (7)$$

where $w_l$ is the desired length of the overlap function that is to be set. The overlapping functions $f[k]$ for the fade-in and $g[k]$ for the fade-out, are required to serve for the purpose of overlapping between two grains, such that the original power is conserved during the overlap.

It is necessary to set the desired length of the overlapping function as a constant for all grains, while also noting that the size of each grain may differ. This is done by setting a constant length $w_l$ for the functions $f[k]$ and $g[k]$ for all the grains, while the variability of the grain lengths are achieved by the length of the unit response between the overlap functions: $N_{unit} = N - 2w_l$.

To be consistent with the length of the overlap functions and the size of the grains, the length $w_l$ is divided equally between the two successive grains. The total length of the window $N$ thus consists of the length of the grain $N(T_{\Delta\beta})$, the length for the preceding overlap $w_l/2$ and the length for the successive overlap $w_l/2$ (Fig. 4). The relation between the length of the window $N$ and the desired length of the overlap function, $w_l$ is thus defined as:

$$w_l/2 + N(T_{\Delta\beta}) + w_l/2 = N \Rightarrow N(T_{\Delta\beta}) + w_l = N_{unit} + 2w_l \Rightarrow w_l = N(T_{\Delta\beta}) - N_{unit}. \qquad (8)$$

This gives us the maximum length of the overlap function $w_l$, that corresponds to the smallest grain in the system and to $N_{unit} = 0$: $w_l = \min(N(T_{\Delta\beta}))$. The length of the overlap function $w_l$ is thus restricted to $0 \leq w_l \leq \min(N(T_{\Delta\beta}))$. The amount of overlap is defined as:

$$\Psi = \frac{w_l}{\min(N(T_{\Delta\beta}))}, \qquad (9)$$

with $0 \leq \Psi \leq 1$. The defined window function for $\Psi = 20\%$ is plotted in Fig. 4a.

For two signals to cross-fade while maintaining the required power level during the transition, the cross-fade functions $g$ and $f$, must satisfy the equation given by (Fink et al. (2016)):

$$f^2 + 2 \cdot f \cdot g \cdot r_{(p_1,p_2)} + g^2 = 1, \tag{10}$$

where $r_{(p_1,p_2)}$ is the correlation coefficient of the two overlapping signals $p_1$ and $p_2$, which is zero for uncorrelated signals and one for completely correlated signals. As we assume that successive grains are uncorrelated, $r_{(p_1,p_2)} = 0$ and Eq. (10) also satisfies the Princen-Bradley criterion (Bäckström (2019)). Following Fink et. al. (2016), a number of functions satisfying these conditions are available for the selection of the cross-fading overlap function. The simplest and efficient functions for the windows are given by $f(\chi) = \sin(\frac{\pi \chi}{2})$ and $g(\chi) = \cos(\frac{\pi \chi}{2})$, where $\chi \in [0,1]$ is the normalized time index. These functions used in Eq. (7), with the desired length of the overlap function $w_l$ determined by Eq. (9) define the window function used to facilitate the cross-fading between two successive grains.
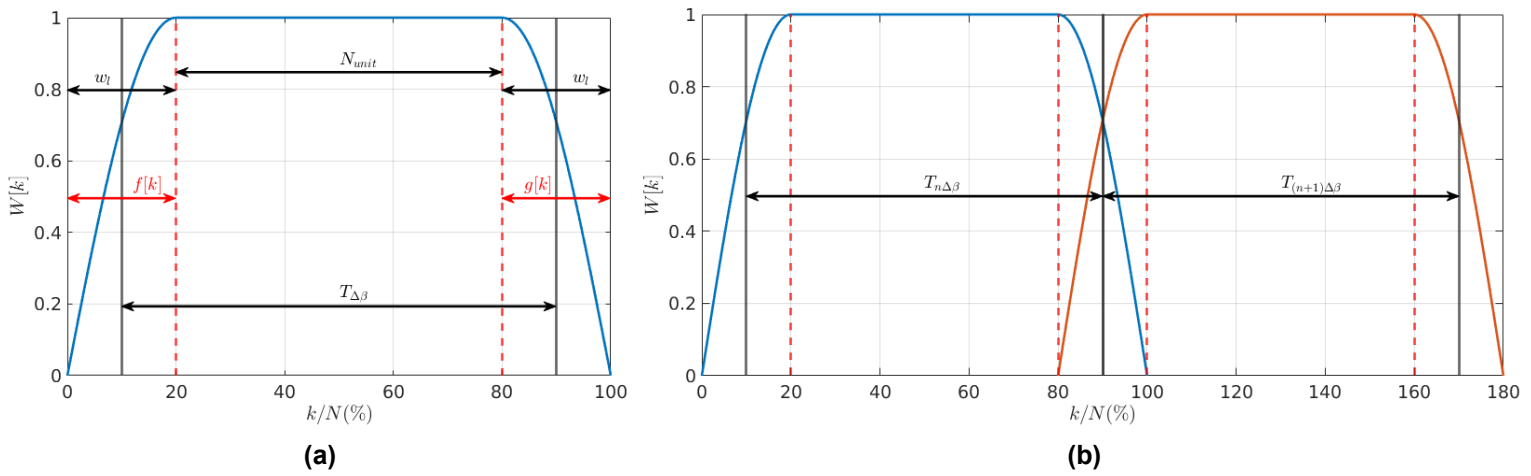


**Figure 4:** (a) The total window function $W[k]$ with the overlapping window functions $f[k]$ and $g[k]$ with $\Psi=20\%$ of overlap (b) Overlap of the window functions.

# 4. Results

## 4.1 Influence of overlap amount in the cross-fading between grains

The principal purpose for the cross-fading window is to facilitate a smoother transition from one grain to the next while maintaining the correct power level. However, the overlap amount determined by $\Psi$, influences the qualitative realism of the auralized signal. To understand the influence of the parameter $\Psi$, a single segment is auralized for the simplest case.

The trailing edge noise emitted by the tip segment of one wind turbine blade at a radial distance of $45$ m, rotational speed $\Omega= 1.47$ rad/sec and hub height of $H_0 = 80$ m is auralized with $N_\beta=12$ discrete angular positions. The wind inflow velocity for all position is taken to be 8 m/s (no wind shear). The maximum change in amplitude of the auralized noise will be observed for a receiver at the crosswind position ($\tau = 90°$). Taking the distance of the receiver as $R_0 = 100$ m from the base of the hub for this position, the system is auralized for different values of $\Psi$, between 1% and 100%.

An RMS with the moving window of duration 50 ms is used to calculate the SPL which is used as an envelope function to detect the structural changes in the auralized signal related to the individual grains. This time duration is well adapted to detect the structural differences in the
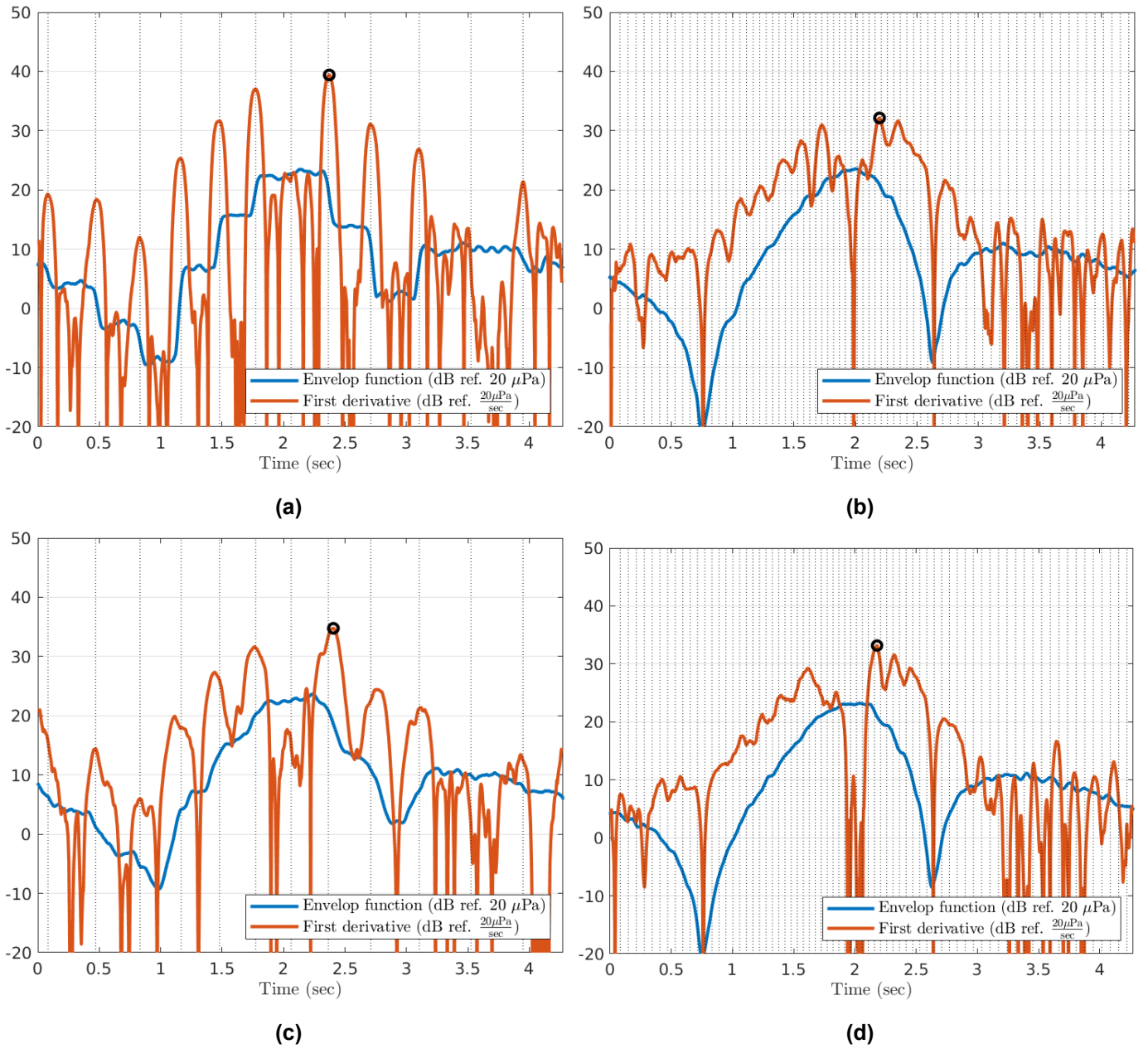
**Figure 5:** The envelope function $L_1(t)$ with the SPL of the time derivative $L_2(t)$. The vertical lines indicate the transitions in time between the grains and the black circle showing the peak of the derivative.
(a) $\Psi = 1\%$ and $N_\beta$= 12, (b) $\Psi = 1\%$ and $N_\beta$= 72, (c) $\Psi = 100\%$ and $N_\beta$= 12, (d) $\Psi = 100\%$ and $N_\beta$= 72.

signal because the minimum grain duration in the system is greater than 50 ms. The SPL of the envelop function used is given by:

$$L_1(t) = 10 \; \log_{10} \left( \frac{p^2_{rms,50\text{ms}}(t)}{p^2_{ref}} \right) \quad \text{(dB re. 20 } \mu\text{Pa)}, \tag{11}$$

where $p_{rms,50\text{ms}}$ is the moving RMS over 50 ms. The change in the amplitude of the grains is understood by taking the SPL of the time derivative of the moving RMS which is given by:

$$L_2(t) = 10 \; \log_{10} \left( \frac{(dp_{rms,50\text{ms}}(t)/dt)^2}{(p_{ref}/1 \; s)^2} \right) \quad \text{(dB re. 20 } \mu\text{Pa/s)}. \tag{12}$$

The variations in the amplitude between successive grains is captured as peaks as seen in Fig. 5. The maximum rate of change in the amplitude in the auralized signal is used to quantify the quality

of the transitions for different amounts of the overlap. For different values of $\Psi$, the maximum rate of amplitude change between grains is seen in Fig. 6a.

The larger the amount of the overlap between two grains, the smoother is the transition, with $\Psi$ = 100% facilitating the smoothest transition between grains. A difference of $\sim 6\ dB$ of the rate of amplitude change is seen between the maximum and minimum values of the overlap. This difference between the change in the amplitudes of each grain for different values of $\Psi$ is clearly audible: [link]. The average SPL calculated by Eq. (11) for the entire signal is the same for every value of $\Psi$ with the standard deviation of less than 1 dB, which indicates that the overall power level is conserved for all values of $\Psi$. As the computational cost is the same for any value of $\Psi$, choosing the optimal amount of $\Psi$ = 100% is beneficial for the synthesis of the signal.
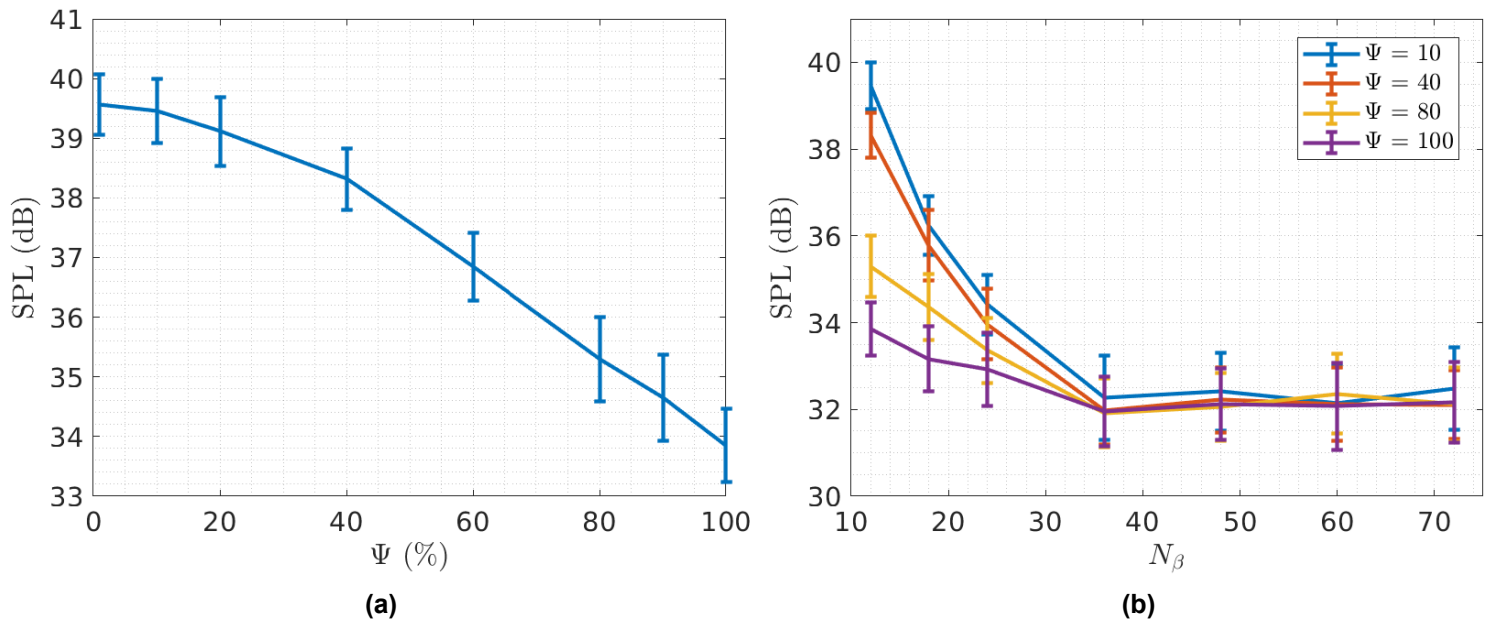


**Figure 6:** Maximum of the calculated SPL $L_2$ for (a) different values of $\Psi$ with $N_\beta = 12$, (b) different values of $N_\beta$. The error bars show the standard deviation calculated over 50 realizations.

## 4.2  Influence of the number of grains

The number of grains in the auralized signal is equal to the number of discrete angular positions $N_\beta$ set for the rotation of the blade. It is apparent that the larger the number of angular positions, the closer the system approaches the continuous rotational motion of the blade. The difference in the amplitude between two adjacent grains changes with the number of discretized angular positions in a single rotation. For a larger number of discretized angular positions, the amplitude change between adjacent grains is less, resulting in a smoother transition between grains in the auralized signal. The influence of $N_\beta$ on the quality of the auralized signal can thus be related to the rate of the amplitude change between grains. To understand how the quality of the auralized signal is influenced by $N_\beta$, the tip segment is considered as in the previous section (Section 4.1) using different values of $N_\beta$.

The SPL of the envelop function as defined by Eq. (11) is taken again over 50 ms which is still smaller than the smallest grain size used for the analysis. The rate of change in the amplitude is captured by taking the SPL of the moving RMS which is defined by Eq. (12). The maximum rate of change in the amplitude of the auralized signal is used to quantify the influence of $N_\beta$ on the quality of the signal. For different values of $N_\beta$, the maximum rate of amplitude change between grains is seen in Fig. 6b. It is clear from Fig. 5 and 6b that the quality of the transitions in the auralized signal is influenced by the number of discrete angular positions, $N_\beta$. The value of the

curves of the maximum rate of change converges for $N_\beta$ greater than 36. This difference of the quality of the transitions is also audibly distinct [link], with the largest value of $N_\beta$ approaching the smoothest signal.

Increasing $N_\beta$ comes with an increase of the computational cost. To resolve this particular trade-off between the realism and computational cost, a lower value of $N_\beta$ can be used with the largest possible value of $\Psi$. Using $N_\beta = 36$ and $\Psi = 100\%$ the signal can be auralized approaching the quality that is attained using $N_\beta = 72$ and $\Psi = 10\%$ [link]. Note that the auralization done for this analysis concerns a single blade segment. Accounting all the segments of the wind turbine blades will induce less audible artifacts, as the transitions of each grain occur at a different time for each segment, thus the transitions between grains are not very noticeable when a complete wind turbine is auralized.

## 4.3 Test cases

Using the optimal values of the parameters $\Psi = 100\%$ with $N_\beta = 36$, we auralize the wind turbine noise for different receiver positions between the frequency limits $f_{min}$= 100 Hz and $f_{max}$= 6000 Hz. As the trailing edge noise and turbulent inflow noise have independent contribution to the noise of the wind turbine, they are auralized separately and then summed together. Similarly the contribution of each of the 8 segments of the blade is considered to be independent and thus also auralized separately and finally summed. The resultant auralized signal from one blade is shifted correspondingly in time to add the response of the second and the third blade of the wind turbine, thus achieving the desired auralization for the wind turbine noise.

For a wind turbine with rotational speed $\Omega$ = 1.47 rad/sec, blade span of 45 m and hub height of $H_0$ = 80 m, the test cases are done for no wind shear and different wind shear exponents, $\alpha$ and various receiver positions on the ground. The turbulence parameters that are considered correspond to a neutral atmosphere, as given in Tian and Cotté (2016). The spectrograms of the auralized signals for the receivers at the downwind and crosswind positions are seen in Fig. 7. Strong amplitude modulation is seen in the crosswind position, while there is less variation downwind. The auralized signals for the test cases of different parameters are available here: `http://sites.google.com/view/david-mascarenhas/wtnc-2021`.
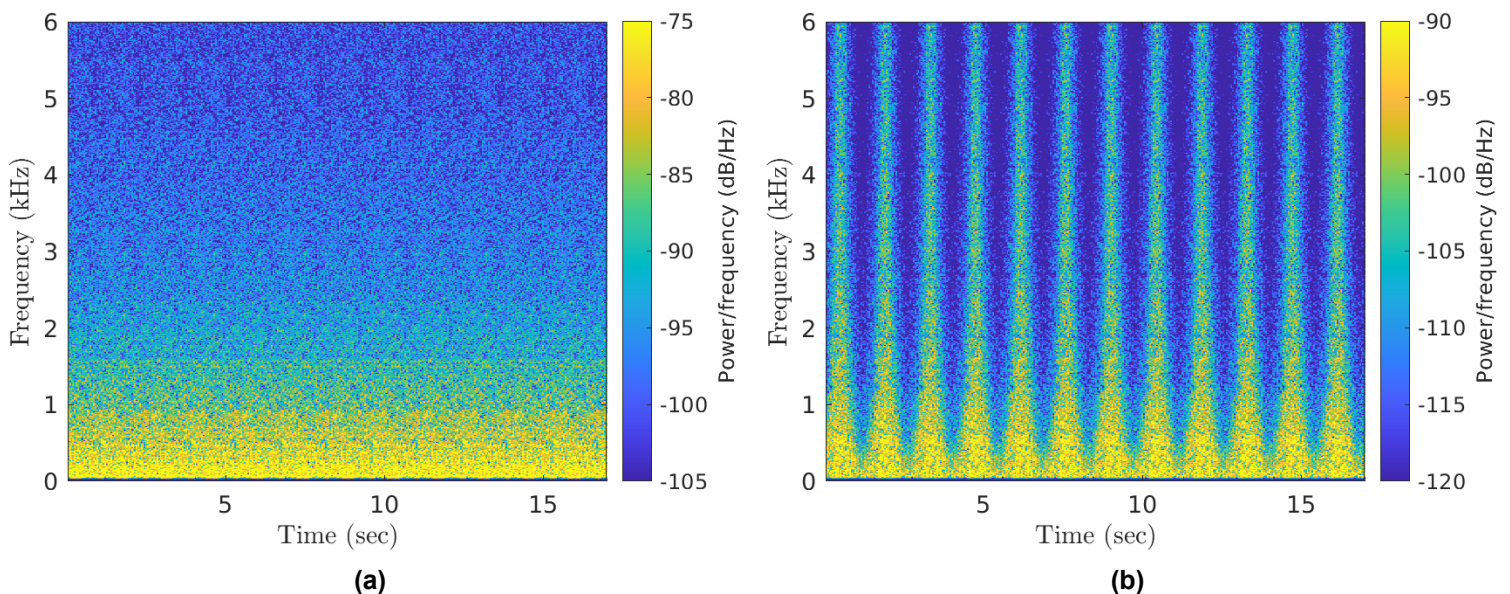


**Figure 7:** The spectrograms of the auralized wind turbine noise inclusive of turbulent inflow noise and trailing edge noise for no wind shear. Receiver position at $R_0$ = 100 m and (a) Downwind ($\tau = 0°$), (b) Crosswind ($\tau = 90°$).

# 5.  Conclusions

The auralization tool discussed in this article converts the frequency-domain model of the wind turbine noise to a time-domain signal.  The auralization is based on the physical models of the airfoil noise generated by the leading edge and the trailing edge of the wind turbine blades. As this model is physics-based, modification in the parameters such as the receiver position, rotational speed, wind speed etc.  are easily achieved to alter the requirements for the desired auralized signal.  The important parameters that alter the quality of the auralization such as the overlap amount $\Psi$ and the number of grains $N_\beta$ are also described. From the analysis, we conclude that the optimum value for $\Psi$ is 100% and induce no additional computational cost. We also conclude that the maximum rate of change in the amplitude for different values of $N_\beta$ converges above $N_\beta$ = 36. Considering the computational cost and the audible difference which is noticeable, $N_\beta$ = 36 and $\Psi$ = 100% provides the optimum values for the auralization.

The auralization is done based on the source emitting the airfoil noise in free field.  This does not include the atmospheric and propagation effects such as absorption, refraction, ground reflection. Other sources of noise such as vegetation and background noise also need to be added to simulate a realistic environment of the required scenario. The estimated values of the parameters that are used are on the basis of the results obtained by signal processing. In the future, we can envisage to optimize the synthesis parameters on the basis of psycho-acoustic analysis in order to minimize computational costs while achieving the most realistic wind turbine auralization.

# Acknowledgement

# References

Amiet, R. K. (1975). Acoustic radiation from an airfoil in a turbulent stream. *Journal of Sound and vibration*, 41(4):407–420.

Amiet, R. K. (1976). Noise due to turbulent flow past a trailing edge. *Journal of sound and vibration*, 47(3):387–393.

Bäckström, T. (2019). Overlap-add windows with maximum energy concentration for speech and audio processing. In *ICASSP 2019-2019 IEEE International Conference on Acoustics, Speech and Signal Processing (ICASSP)*, pages 491–495. IEEE.

Bertagnolio, F., Madsen, H. A., and Fischer, A. (2017).  A combined aeroelastic-aeroacoustic model for wind turbine noise: verification and analysis of field measurements.  *Wind Energy*, 20(8):1331–1348.

Bowdler, D. and Leventhall, G. (2011).  *Wind Turbine Noise: how it is produced, propagated measured and received*. Multi-Science Publishing, Brentwood, UK.

Buck, S., Oerlemans, S., and Palo, S. (2018). Experimental validation of a wind turbine turbulent inflow noise prediction code. *AIAA Journal*, 56(4):1495–1506.

Fink, M., Holters, M., and Zölzer, U. (2016). Signal-matched power-complementary cross-fading and dry-wet mixing. *Proceedings of the 19th International Conference on Digital Audio Effects (DAFx-16)*.

Oerlemans, S. and Schepers, J. G. (2009). Prediction of wind turbine noise and validation against experiment. *International journal of aeroacoustics*, 8(6):555–584.

Pieren, R., Heutschi, K., Müller, M., Manyoky, M., and Eggenschwiler, K. (2014). Auralization of wind turbine noise: emission synthesis. *Acta Acustica United with Acustica*, 100(1):25–33.

Roger, M. and Moreau, S. (2010). Extensions and limitations of analytical airfoil broadband noise models. *International Journal of Aeroacoustics*, 9(3):273–305.

Sinayoko, S., Kingan, M., and Agarwal, A. (2013). Trailing edge noise theory for rotating blades in uniform flow. *Proceedings of the Royal Society A: Mathematical, Physical and Engineering Sciences*, 469(2157):20130065.

Tian, Y. and Cotté, B. (2016). Wind turbine noise modeling based on amiet's theory: Effects of wind shear and atmospheric turbulence. *Acta Acustica united with Acustica*, 102(4):626–639.